Metabolic Cost of Rapid Adaptation of Single Yeast Cells Under Unforeseen Challenge

Gabrielle Woronoff[1,2,§], Philippe Nghe[2,§], Jean Baudry[1], Laurent Boitard[1], Erez Braun[3], Andrew D. Griffiths[2]*, and Jérôme Bibette[1]*.

[1]Laboratoire de Colloïdes et Matériaux Divisés (LCMD) and [2]Laboratoire de Biochimie (LBC), ESPCI Paris, PSL University, CNRS UMR8231, Paris, France. [3]Department of Physics & Network Biology Research Laboratories, Technion, Haifa, Israel.

[§]These authors contributed equally
*e-mail: andrew.griffiths@espci.fr and jerome.bibette@espci.fr
Keywords: single cell metabolism, droplet-based microfluidics, genetic rewiring, adaptation

Introductory paragraph

Cells are known to be able to adapt to changing environments. In the classical neo-Darwinian picture, random genetic mutations cause phenotypic variations, enabling adaptation to the new environment. In addition, non-genetic pathways are increasingly believed to play an important role in rapid adaptation, notably in the emergence of drug resistance[1-7]. However, the coupling between metabolism and adaptation has never been addressed at the single-cell level. Here we show that following a severe, unforeseen challenge, yeast cells display a wide range of metabolic rates, and can adapt rapidly, with the rate of adaptation being controlled by the metabolic rate. We simultaneously measured metabolism and division of thousands of individual *Saccharomyces cerevisiae* cells, using a droplet-based microfluidic system[8]. Remarkably, the majority (~88%) of the cells, while not dividing, nevertheless displayed a metabolic response with a wider diversity of metabolic rates (CV=0.60) than unchallenged cells (CV=0.24). Over the course of the 70 h experiment, a sizeable fraction of cells (53%) switched state either by accelerating their metabolism (4%, metabolic recovery) or arresting it (49%). The time of acceleration was inversely proportional to the initial metabolic rate and a large fraction (73%) of these recovering cells resumed division, on average at the same time they accelerate their metabolism. This indicates that adaptation is an active process, requiring the consumption of a characteristic amount of energy. The adaptation rate (10^{-3}cells/h) is orders of magnitude higher than expected based on known mutation rates, suggesting an epigenetic origin. The demonstration that metabolic trajectories predict *a priori* adaptation events offers the first evidence of the tight energetic coupling between the metabolic and regulatory processes in adaptation. This process allows *S. cerevisiae to* adapt on a physiological time scale, but related phenomena may also be important in other processes, such as cellular differentiation, cellular reprogramming and the emergence of drug resistance in cancer.

Text

To investigate adaptation of the yeast *S. cerevisiae* confronted with a severe environmental challenge, we genetically "rewired" cells by detaching the essential *HIS3* gene of the histidine biosynthesis system from its native regulatory system and placed it under the exclusive regulation of the *GAL* system responsible for galactose metabolism[9]. The *GAL* system is highly induced in the presence of galactose and strongly repressed in glucose. Switching cells from galactose to glucose in a medium lacking histidine presents the yeast with the challenge of reinitiating histidine synthesis in order to resume growth and prevent extinction. The population dynamics of this system have previously been studied in detail by Braun and coworkers[9-15]. After switching to glucose, growth continues for ~1 day (Phase I) then, after a few days with little or no growth (Phase II), normal growth is resumed at the population level (Phase III) with a doubling time similar to that before the challenge, indicating that after only a few days the population is fully adapted (Fig. 1).

To track adaptation at the single-cell level, we used a droplet-based microfluidics system that allows simultaneous measurements of growth and metabolism of a large number (several thousands) of single yeast cells over time[8]. Individual cells, harvested from batch cultures 3 h after the beginning of Phase II (Fig. 1; green triangle), were compartmentalized in 30 pL droplets and incubated at 30°C in a closed glass observation chamber for 65 to 70 h (Fig. 2a). The concentration of cells was set so that only a small fraction of the droplets contains single cells (typically 6%), and these are surrounded by empty droplets. The consumption of nutrients (glucose) in a cell-containing droplet creates an osmotic imbalance, resulting in an osmotically driven water flux, which induces the shrinkage of this droplet and the swelling of neighboring cell-free droplets (Supplementary Video 1). For each experiment, images were taken every 20 or 30 minutes during 3 days and used to determine the change in volume of each droplet as a function of time, reflecting cell metabolism, while simultaneously imaging the cells themselves to measure their division (Methods). Three independent batch cultures were analyzed (Methods); however, hereafter, only the consolidated data from these three independent experiments is plotted and analyzed (see Supplementary Table 1 for analysis of individual experiments).

Metabolic activity was detectable for 88% of cells (final droplet volume <0.95 of initial volume, see Methods, Extended Data Fig. 1). The volume variation of droplets containing cells displaying metabolic activity is plotted for both the control experiment, with histidine in the medium (Fig. 2b), and the adaptation experiment, in the absence of histidine (Fig. 2c). Cells in medium lacking histidine showed remarkably diverse metabolic trajectories (CV = 0.60 at 10 hours), while in the presence of histidine the diversity of the metabolic trajectories was more restricted (CV = 0.24 at 10 hours, Extended Data Fig. 2) and similar to wild-type yeast[8]. Consistent with these results, earlier studies in bulk showed a wide diversity of gene expression profiles in cells from Phase II[12].

Quantitative analysis of the change of single droplet volumes over time (Extended Data Figures 1-5) demonstrated two important switching events within the population of metabolizing cells (Fig. 2d): (i) "metabolic arrests" in which the volume curve flattened before nutrient exhaustion and (ii) "metabolic recoveries" in which the shrinkage rate increased to a similar level as for cells under non-stressed conditions (in the presence of histidine). Cells which fall in neither of these two categories are termed "steady metabolisms". The time of metabolic arrest (T_{arr}) and time of

metabolic recovery (T_{rec}) were determined as respectively the minimum and the maximum of the second derivative of the drop-shrinkage curves (arrowheads in Fig. 2d, Methods).

The population of metabolically arrested cells was characterized by a final volume plateau, at a value larger than the final volume of cells grown with histidine (Fig. 2e,f). In the presence of histidine, an abrupt decrease in metabolic rate was reached when glucose in the droplet was exhausted by the cells[8], corresponding to a mean final droplet volume of 0.49±0.002 of the initial value, and always <0.55 of the initial value (Fig. 2e, red). In contrast, in the adaptation experiment in the absence of histidine (Fig. 2e, blue), 54% of cells had a final volume >0.55 of the initial value, indicating that they had not consumed all the glucose in the droplet. These cells fall into two categories. In the first category are cells (49%) that arrested their metabolism during the experiment (Fig. 2f), as they were initially metabolically active and showed an abrupt metabolic deceleration and a stable volume, indicating that the cells were not metabolically active from that point in time (T_{arr}). A second category of cells (5%) neither arrested, nor recovered, but had a metabolism slow enough that glucose was not exhausted at the end of the experiment.

Metabolic recoveries in the adaptation experiment were determined as those cells whose metabolic rate increased to levels comparable to the control with histidine, as computed by the difference between the maximum rate (R_{max}) and the initial rate (R_0) (2 hours after compartmentalization) obtained from the volume time course of each droplet (Fig. 2g). In the control, the metabolic rate of cells steadily increased due to cell growth and division before glucose exhaustion (Fig. 2b)[8], with a mean rate increase of 3.6±0.7 10^{-2} h^{-1} (Fig. 2g, red). In the adaptation experiment, 4% of cells accelerated their metabolic rates (N=120, Fig. 2h) to values similar to those observed in the control (>1.3 10^{-2} h^{-1}), the threshold for significant metabolic increase being determined by the overlap between the distributions with and without histidine (red and blue, respectively, in Fig. 2g, Extended Data Fig. 4). The cells that were not part of any of the categories mentioned above (arrested, non-exhausted, recovered) had a steady metabolism until glucose exhaustion (30%).

We next addressed the question of the correlation between metabolic profiles and adaptation — the resumption of division. Each metabolizing cell within the shrinking drops was visualized to determine if division occurred at least once and at what time; the time of division T_{div} being defined as the time of appearance of a first bud eventually leading to a division event. We found that within the subset of cells showing steady metabolism, only about 9% of the cells resumed division, whereas within the metabolic recovery class, about 73% resumed division (Fig. 3a,b). Plotting the distribution of the time difference between the onset of cell division (T_{div}) and metabolic recovery (T_{rec}) shows that the two events are strongly correlated (R^2=0.79, $p<10^{-5}$, Extended Data Fig. 6), with a mean value $T_{div} - T_{rec} \approx -1.35 \pm 5.5$ h (Fig. 3c), which is significantly smaller than the average time of recovery (29 h). This indicates that division starts when the maximum metabolic acceleration is reached.

We then examined the kinetics within the population of the following events: metabolic arrests, metabolic recoveries and adaptation. The cumulated fraction of metabolic recoveries displayed a sigmoidal shape (Fig. 4a, green), with a quadratic increase up to 30 hours, followed by a leveling off. As expected from the close correlation between the times of metabolic recovery (T_{rec}) and division (T_{div}) (Fig. 3c), the cumulative fraction of cells re-commencing division (Fig. 4a, red)

paralleled the cumulative fraction of cells showing metabolic recovery (Fig. 4a, green). Therefore, the instantaneous rate of adaptation increased over time up to 30 hours where it reached a value of about 10^{-3} cells/hour (Fig. 4b). The recovery time (T_{rec}) as a function of the inverse initial metabolic rate (R_0^{-1}), shows a clear linear correlation (R^2=0.33, $p<10^{-3}$, Fig. 4c). The droplet volume on recovery peaks at ~74% of the initial droplet volume (Fig. 4d, Supplementary Table 1), indicating that on average a characteristic amount of glucose (156 pg) is required for a cell to adapt (Methods). This is equivalent to approximately one day of maintenance energy consumption in wild-type yeast in G1 phase[8]. The consumption of a characteristic amount of glucose for adaptation implies that the distribution of adaptation times is governed by the distribution of the initial metabolic rates. Indeed, the distribution of initial metabolic rates peaks at low values (Fig. 4e), and there are more slower than faster metabolizing cells, which accounts for the increase in the instantaneous recovery rate at early times (Fig. 4g). At later times, the instantaneous recovery rate decreases due to the vanishing number of very slowly metabolizing cells, as well as the competing process of metabolic arrest, the rate of which increases over time, as described below.

In contrast, the cumulated fraction of metabolic arrests increases quadratically throughout the course of the experiments (Fig. 4f), with an acceleration coefficient of 1.01±0.01 $\times 10^{-4}$ $cell^{-1}.h^{-2}$, and the instantaneous death rate increases with time (Fig. 4g). The time of metabolic arrest is poorly correlated with the initial metabolic rate (R^2=0.12, $p<10^{-3}$, Fig. 4h), in agreement with an age driven mechanism essentially independent of the initial metabolic rate.

We finally examined the metabolism of single cells in the adapted populations (Extended Data Fig. 7), taken 2, 4 and 7 days after the batch population entered Phase III (Fig. 1; blue arrows, Supplementary Movie 2). The overall dynamics of the adapted population (Extended Data Fig. 7a), is highly comparable with cells in the absence of stress (Fig. 2b), with a similar spread of final droplet volumes (Extended Data Fig. 7b) and metabolic rates (Extended Data Fig. 7c, CV=0.35 for adapted compared to CV=0.24 for non-stressed cells). The proportions of the different classes of cells are very similar at the three time points: non-metabolizing cells (1.6±1%), non-dividing metabolizing cells (10±1%) and dividing cells (89±2%) (Extended Data Fig. 7d). Consistent with adaptation observed at the population level, the fraction of dividing cells is >10-fold higher than at the beginning of Phase II[10]. The variance in metabolic rate of the dividing cells is similar in the samples taken 2, 4 and 7 days after entering the adapted phase (CV = 0.33±0.04) and very close to that observed for control cells switched to glucose plus histidine (CV = 0.28). None of the 174 dividing cells analyzed reduced their metabolic rate during the droplet-based experiment, demonstrating stability of the adapted state over days at the single cell level, consistent with results at the population level[10,14].

In conclusion, this work establishes the existence of a phenomenon in yeast that allows rapid adaptation and necessitates consumption of a characteristic amount of energy, causing certain cells which metabolize more efficiently to adapt more rapidly. In contrast to persister cells in bacteria, yeast, fungi, parasites and cancer, which are thought to be rare cells (rarely more than 1%, even taking into account the increased fraction of persister cells that may result from stress-induced responses[3]) that lie metabolically dormant and then regrow when the challenge is removed[2-4], we observed here that, shortly after challenge the majority (88%) of cells were metabolizing (but not dividing) and displayed a high diversity of metabolic rates. Furthermore, adaptation, characterized by simultaneous acceleration of metabolism and resumption of division, occurred while the challenge was maintained. The adapted state was stable over the time course of the experiment, backing up

previous observations in bulk, which indicated that the adapted state is stably inherited across generations[9,14], and indicating that this is a genuine adaptation process.

What might explain this finding at a molecular level? The high rate of adaptation is difficult to explain using established genetic mechanisms: stress can increase the mutation rate[16] but the adaptation rate observed here is ~10^{-3} h^{-1}, which is 2 to 6 orders of magnitude higher than the spontaneous reversion rates by point mutation in quiescent histidine auxotrophic yeast cells in the absence of histidine (10^{-5} to 10^{-9} h^{-1})[17], and very high compared to the overall estimated rate of mutation (~10^{-8} per site per generation)[18] and the rate of adaptive mutation (~10^{-11} per generation)[16] in *S. cerevisiae*. This analysis is consistent with previous measurements[11]. This may point to an epigenetic mechanism, driven by a complex interplay between chromatin organisation and transcription factor networks that can transmit altered states to daughter cells, providing heritability and allowing selection, as recently suggested for a similar engineered yeast system[19].

It is known that chromatin states and transcription factor networks are intimately linked to metabolism, and that they can be modified by external stresses[20]. Stress-induced responses are well known in *S. cerevisiae*[21], and entail large-scale changes in gene expression[21], histone modification and chromatin organization[22]. However, consistent with previous results[12], the adaptation process observed here appears to differ from known *S. cerevisiae* stress responses, including the response to amino-acid starvation[23], in a number of ways. Known stress responses are rapid and transient (with changes in gene expression typically peaking after <2 hours)[21,24], and all cells respond broadly similarly[24]. In contrast, the characteristic timescale of adaptation of single cells that that we observe is much longer (~10^3 hours, see Fig. 4b) and only a fraction of cells adapt.

Furthermore, the adaptation process is not simply the result of an epigenetic perturbation allowing access to a novel phenotype(s), due to induction of a permissive or "plastic" state that, for example in cancer, is proposed to allow stochastic oncogene activation or non-physiological cell fate transitions[25]. Instead, adaptation is an active process, requiring the consumption of energy, which implies an active exploration of different states, and fixation of the solution(s) that allow adaptation. Indeed, it has been proposed previously that adaptation of yeast to an unforeseen challenge may involve dynamic exploration of different regulatory states[15]. However, if this is the case, the mechanism by which exploration is triggered and the way the adapted state is fixed allowing inheritance of the adapted state, remains unknown[9,12,14]. Nevertheless, it is clear from our work that adaptation is intimately coupled to cellular metabolism and depends on metabolic efficiency.

The process we describe allows *S. cerevisiae to* adapt on a physiological time scale, and may provide a significant evolutionary advantage, allowing yeast to better survive and adapt faced with a range of environmental challenges. However, it is tempting to speculate that a related process may also play a role in a range of other important processes, including normal cellular differentiation and development. Indeed, stochastic processes, associated with fluctuations in expression of Nanog and other key transcription factors at the single-cell level, have been proposed to play an important role in early stage embryonic stem cell differentiation[26-28]. Likewise, in cancer, epigenetic mechanisms are increasingly believed to play an important role the development, progression and emergence of drug resistance in cancer[25,29]. Furthermore, it may have implications for important biotechnologies, such as reprogramming of human somatic cells to generate induced Pluripotent Stem Cells (iPSCs), which is characterized by a prolonged early stochastic phase, marked by the random and gradual

expression of pluripotency genes[30]. Further investigation may thus lead to important fundamental insights into the process of cellular differentiation as well as non-genetic mechanisms of adaptation and may have important practical applications such as combating drug resistance in cancer and improving the efficiency of tissue engineering and cellular reprogramming.

Acknowledgments

The authors thank Paul M. Chaikin (New York University) for helpful discussions. EB acknowledges support from a NSF-BSF grant (#2014713).

Author Contributions

G.W., P.N., J.Baudry, L.B., E.B., A.D.G. and J.Bibette designed the study; G.W. performed the experiments; G.W. and P.N. analyzed the data; G.W., P.N., J.Baudry, E.B., A.D.G. and J.Bibette interpreted the data and wrote the paper.

Competing Interests

The authors declare no competing interests.

Additional Information

Supplementary information is available for this paper

Correspondence and requests for materials should be addressed to A.D.G. or J.B.

References

1 Bigger, J. Treatment of staphylococcal infections with penicillin by intermittent sterilisation. *Lancet* **244**, 497-500 (1944).

2 Lewis, K. Persister cells, dormancy and infectious disease. *Nat. Rev. Microbiol.* **5**, 48-56 (2006).

3 Cohen, N. R., Lobritz, M. A. & Collins, J. J. Microbial Persistence and the Road to Drug Resistance. *Cell Host and Microbe* **13**, 632-642 (2013).

4 Verstraeten, N., Knapen, W., Fauvart, M. & Michiels, J. Bacterial Persistence: Method and Protocols. Vol. 1333 (Springer Science + Business Media, 2016).

5 Sharma, S. V. *et al.* A chromatin-mediated reversible drug-tolerant state in cancer cell subpopulations. *Cell* **141**, 69-80 (2010).

6 Lackner, M. R., Wilson, T. R. & Settleman, J. Mechanisms of acquired resistance to targeted cancer therapies. *Fut. Medicine* **8**, 999-1014 (2012).

7 Levin-Reisman, I. *et al.* Antibiotic tolerance facilitates the evolution of resistance. *Science* **355**, 826-830 (2017).

8 Boitard, L. *et al.* Monitoring single-cell bioenergetics via the coarsening of emulsion droplets. *Proc. Natl. Acad. Sci. USA* **109**, 7181-7186 (2012).

9 Stolovicki, E., Dror, T., Brenner, N. & Braun, E. Synthetic gene recruitment reveals adaptive reprogramming of gene regulation in yeast. *Genetics* **173**, 75-85 (2006).

10 Moore, L. S., Stolovicki, E. & Braun, E. Population dynamics of metastable growth-rate phenotypes. *PloS One* **8**, e81671 (2013).

11 Moore, L. S. *et al.* Induced mutations in yeast cell populations adapting to an unforeseen challenge. *PLoS One* **9**, e111133 (2014).

12 Stern, S., Dror, T., Stolovicki, E., Brenner, N. & Braun, E. Genome-wide transcriptional plasticity underlies cellular adaptation to novel challenge. *Mol. Systems Biol.* **3**, 106 (2007).

13 Stolovicki, E. & Braun, E. Collective dynamics of gene expression in cell populations. *PloS One* **6**, e20530 (2011).

14 David, L., Stolovicki, E., Haziz, E. & Braun, E. Inherited adaptation of genome-rewired cells in response to a challenging environment. *HFSP J.* **4**, 131-141 (2010).
15 Braun, E. The unforeseen challenge: from genotype-to-phenotype in cell populations. *Rep. Prog. Phy.*, 78, 036602 (2015).
16 Zeyl, C. Capturing the adaptive mutation in yeast. *Res. Microbiol.* **155**, 217-223 (2004).
17 Hall, B. G. Selection-induced mutations occur in yeast. *Proc. Natl. Acad. Sci. USA* **89**, 4300-4303 (1992).
18 Kondrashov, F. A. & Kondrashov, A. S. Measurements of spontaneous rates of mutations in the recent past and the near future. *Phil. Trans. Roy. Soc. B: Biological Sciences* **365**, 1169-1176 (2010).
19 Freddolino, P. L., Yang, J., Momen-Roknabadi, A. & Tavazoie, S. Stochastic tuning of gene expression enables cellular adaptation in the absence of pre-existing regulatory circuitry. *eLife* **7**, 393 (2018).
20 Sharma, U. & Rando, O. J. Metabolic Inputs into the Epigenome. *Cell Metabolism* **25**, 544-558 (2017).
21 Gasch, A. P. *et al.* Genomic expression programs in the response of yeast cells to environmental changes. *Mol. Biol. Cell* **11**, 4241-4257 (2000).
22 Weiner, A. *et al.* High-Resolution Chromatin Dynamics during a Yeast Stress Response. *Mol. Cell* **58**, 371-386 (2015).
23 Natarajan, K. *et al.* Transcriptional Profiling Shows that Gcn4p Is a Master Regulator of Gene Expression during Amino Acid Starvation in Yeast. *Mol. Cell. Biol.* **21**, 4347-4368 (2001).
24 Zhang, R. *et al.* High-throughput single-cell analysis for the proteomic dynamics study of the yeast osmotic stress response. *Scientific Reps.*, 1-10 (2017).
25 Flavahan, W. A., Gaskell, E. & Bernstein, B. E. Epigenetic plasticity and the hallmarks of cancer. *Science* **357** (2017).
26 Kalmar, T. *et al.* Regulated fluctuations in nanog expression mediate cell fate decisions in embryonic stem cells. *PLoS Biol.* **7**, e1000149 (2009).
27 MacArthur, B. D. & Lemischka, I. R. Statistical mechanics of pluripotency. *Cell* **154**, 484-489 (2013).
28 Stumpf, P. S. *et al.* Stem Cell Differentiation as a Non-Markov Stochastic Process. *Cell Systems* **5**, 268-282.e267 (2017).
29 Salgia, R. & Kulkarni, P. The Genetic/Non-genetic Duality of Drug 'Resistance' in Cancer. *Trends Cancer* **4**, 110-118 (2018).
30 Buganim, Y., Faddah, D. A. & Jaenisch, R. Mechanisms and models of somatic cell reprogramming. *Nat. Rev. Genetics* **14**, 427-439 (2013).

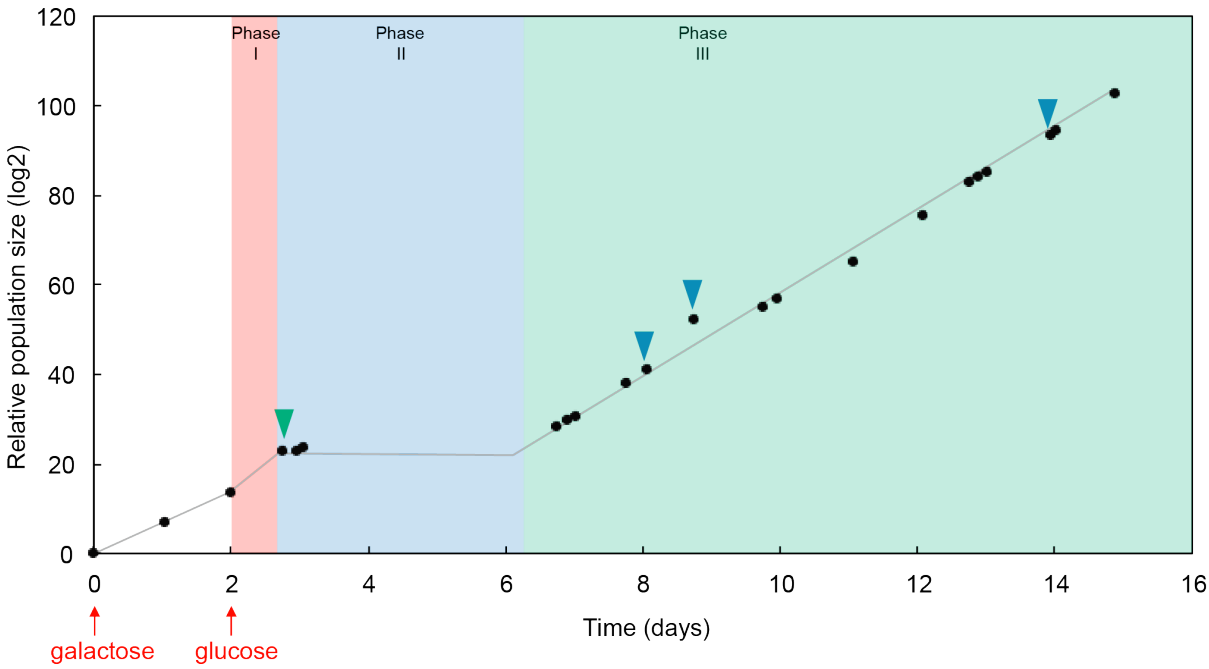

Figure 1. Population growth of naïve rewired cells propagated in bulk cultures throughout the whole process of adaptation. Experiment 1. The culture started with galactose as sole source of carbon (first red arrow). Then, the medium is switched to glucose (second red arrow). The culture continues to grow during the "initial growth phase" (phase I), before entering the "latent phase" (phase II) where the culture does not grow anymore. Finally, the population grows again, entering the "adapted phase" (phase III). Green and blue triangles indicate time points when samples were taken for analysis in droplets (green triangle: 3 hours after the beginning of phase II; blue triangles: 2, 3 and 6 days after the onset of phase III).

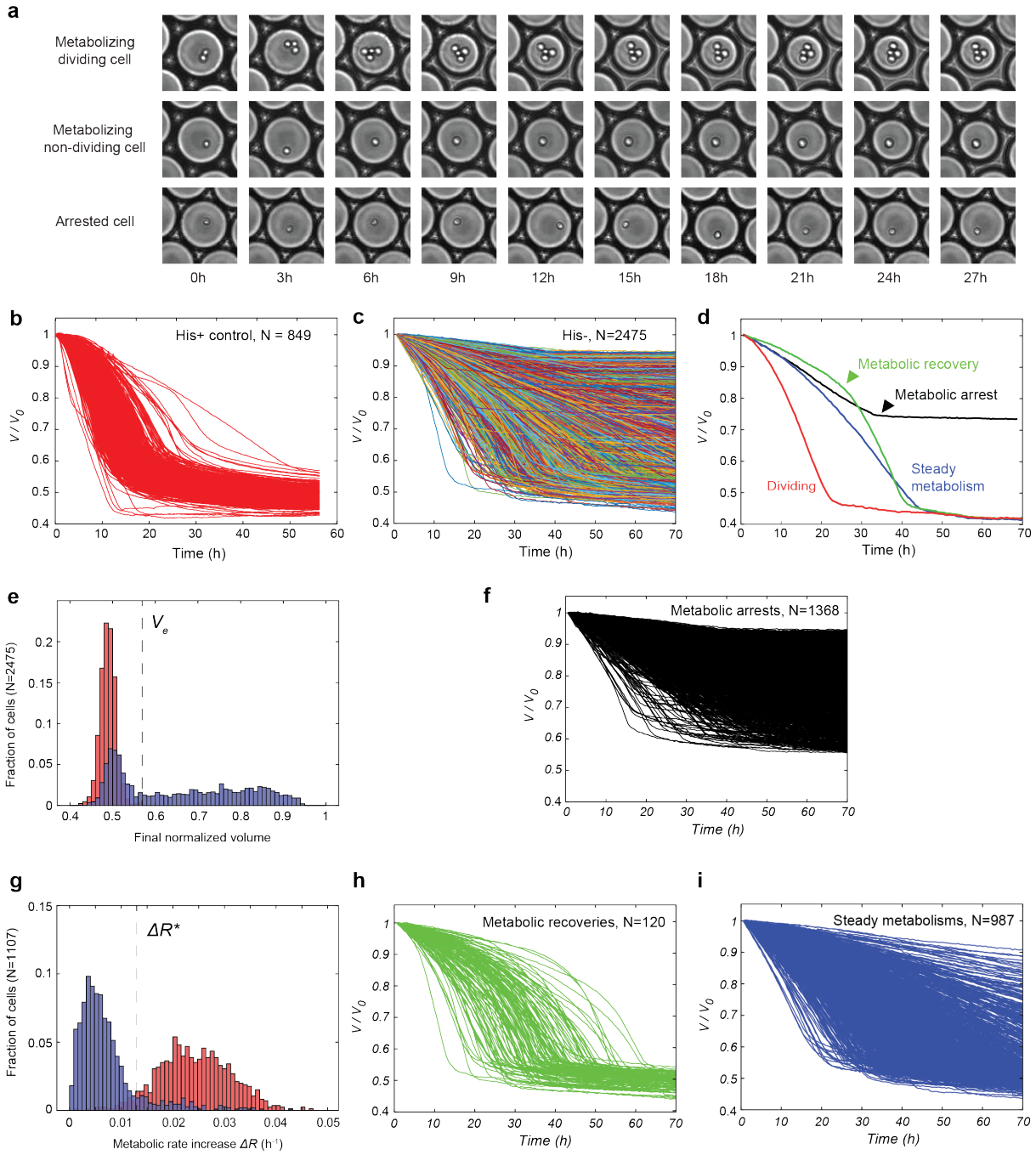

Figure 2. Single-cell analysis of metabolic dynamics in droplets. a) Time-lapse sequences of droplets containing single cells, from top row to bottom row: metabolizing dividing, metabolizing non-dividing and arrested cells. b) Single droplet volume traces of the droplet volume V normalized by the initial volume V_0 in the absence of metabolic challenge, histidine being provided in the medium. c) Single droplet volume traces starting 3 hours after switching from galactose to glucose. Lines are color coded as for panel d. d) Examples of volume traces of single droplets initially containing a single cell for each category of response, depending on the change of metabolic and division states. e) Distribution of final droplet volume (V_f) normalized by the initial volume (V_0) in the presence (red) and absence (blue) of histidine. V_e indicates the maximum volume reached in the absence of challenge. f) Subset of arrested metabolisms from panel b. g) Distributions of the difference ΔR (metabolic rate increase) between the initial (at 2 hours) and maximum metabolic rates in the presence (red) and absence (blue) of histidine. ΔR^* indicates the cross-over between distributions of

metabolic rate increase in stressed (no histidine) and non-stressed (with histidine) conditions. h) Subset of metabolic recoveries from panel b. i) Subset of steady metabolisms from panel b.

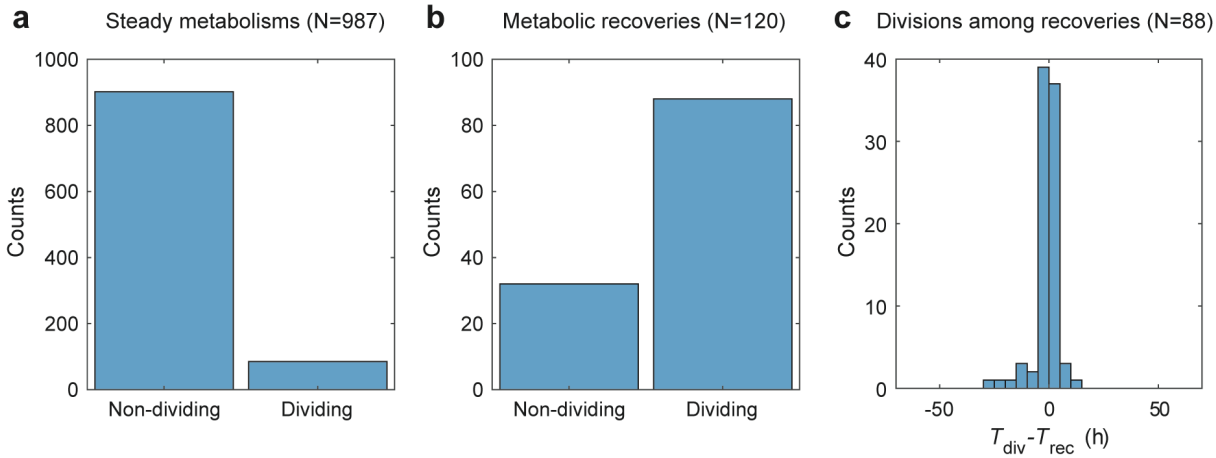

Figure 3. Relation between onset of division and metabolic recovery. a) Fraction of dividing cells in steady metabolisms. b) Fraction of dividing cells in metabolic recoveries. c) Distribution of the difference between division time (T_{div}) and metabolic recovery time (T_{rec}).

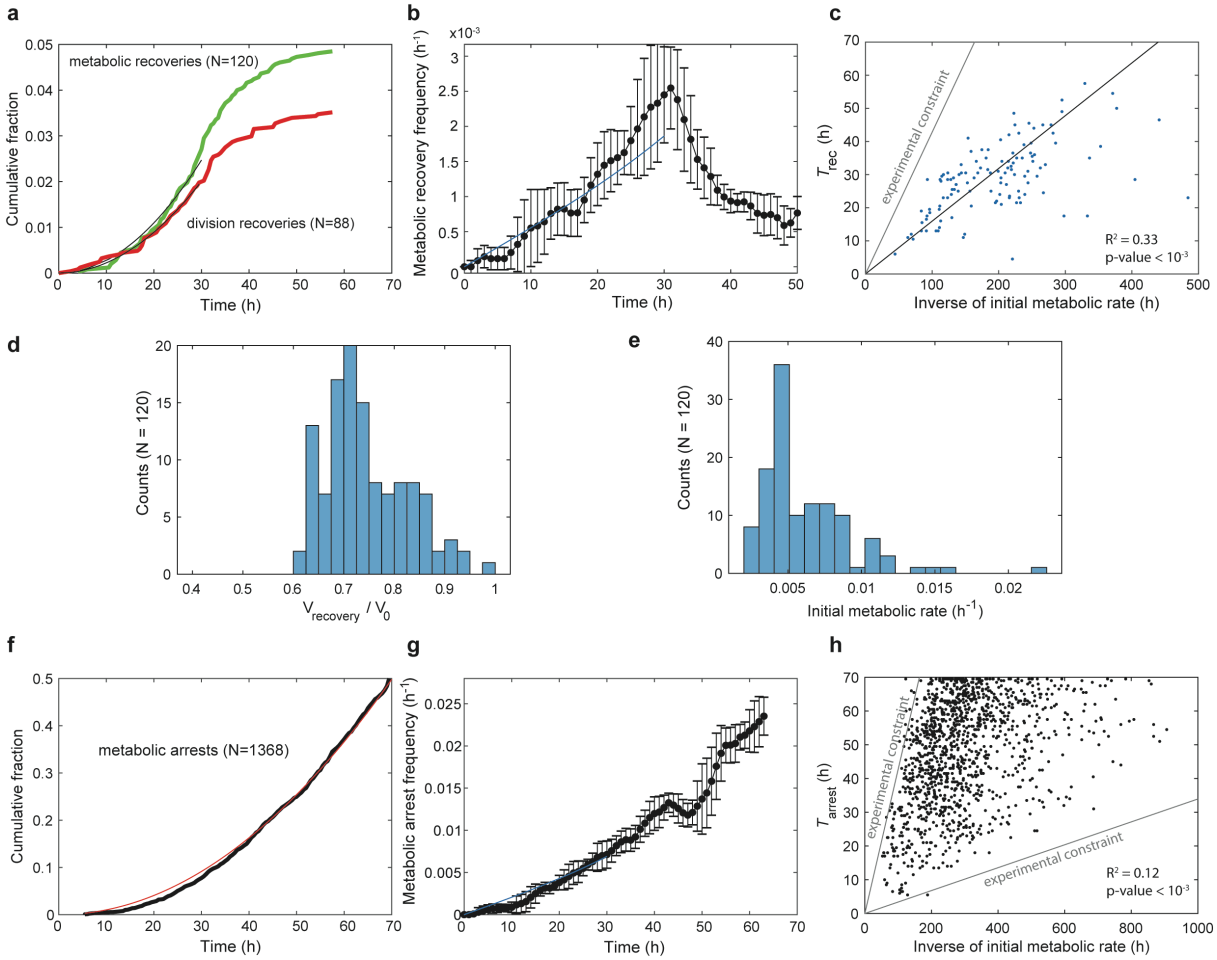

Figure 4. Characterization of adaptation. a) Cumulative fraction over time for metabolic recoveries (green) and division recoveries (red). Black lines are a quadratic fit over the first 30 hours. b) Instantaneous frequency of recoveries over cells that have neither arrested their metabolism nor already recovered. At each time point, frequencies are computed over 7 consecutive points and error bars are standard deviations over the values obtained over these points. The light blue line is the frequency computed from the quadratic fits of panels a and f. c) Correlation between the characteristic time of initial metabolisms (inverse of initial metabolic rate) and the time of recovery. The parameter region above the grey line corresponds to cells that have exhausted droplet resources before being able to recover. The contribution of this constraint has been accounted for to compute the coefficient of determination R^2 (Methods). d) Distribution of normalized droplet volume at the time of recovery. e) Distribution of initial metabolic rate for the sub-population of metabolic recoveries. f) Cumulative fraction over time for metabolic arrests (black). The red line is a quadratic fit over the full time course. g) Instantaneous frequency of arrests over cells that have neither recovered nor already arrested their metabolism, computed as in panel b. The light blue line is the frequency computed from the quadratic fits of panels a and f. h) Correlation between the characteristic time of initial metabolisms (inverse of initial metabolic rate) and the time of arrest. The parameter region above the upper grey line corresponds to cells that have exhausted droplet resources before arresting. The parameter region below the lower grey line corresponds to curves whose final volume is indistinguishable from curves of empty droplets (overall volume variation<5%). The contribution of these constraints has been accounted for to compute the coefficient of determination R^2 (Methods).

Extended Data

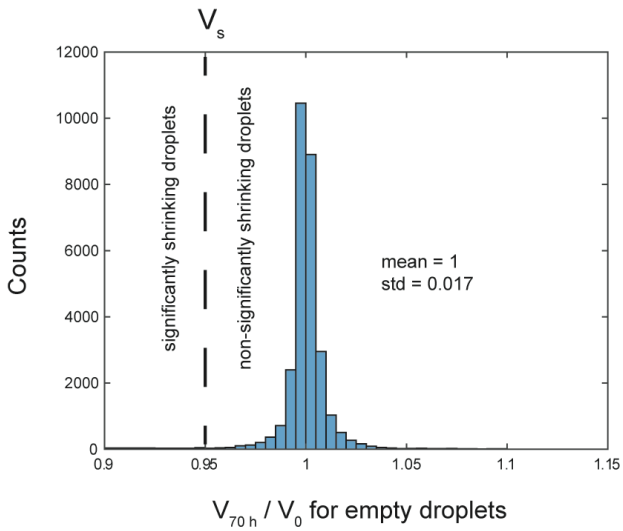

Extended Data Figure 1. Threshold for significant shrinking. The threshold V_s = 0.95 for maximal final volume indicating a significant volume decrease is defined as 3 standard deviation away from the mean of volume distribution of empty droplets.

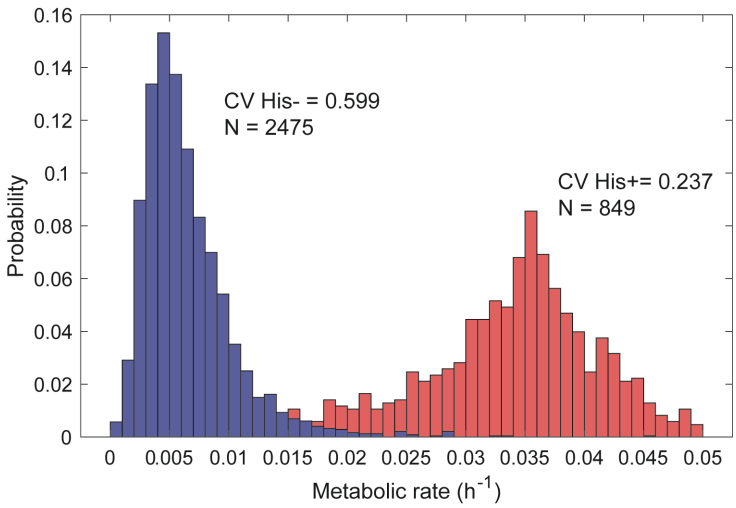

Extended Data Figure 2. Distribution of metabolic rates at 10 hours after encapsulation of yeast in droplets. Red: in the absence of metabolic challenge (with histidine). Blue: in response to a metabolic challenge (no histidine).

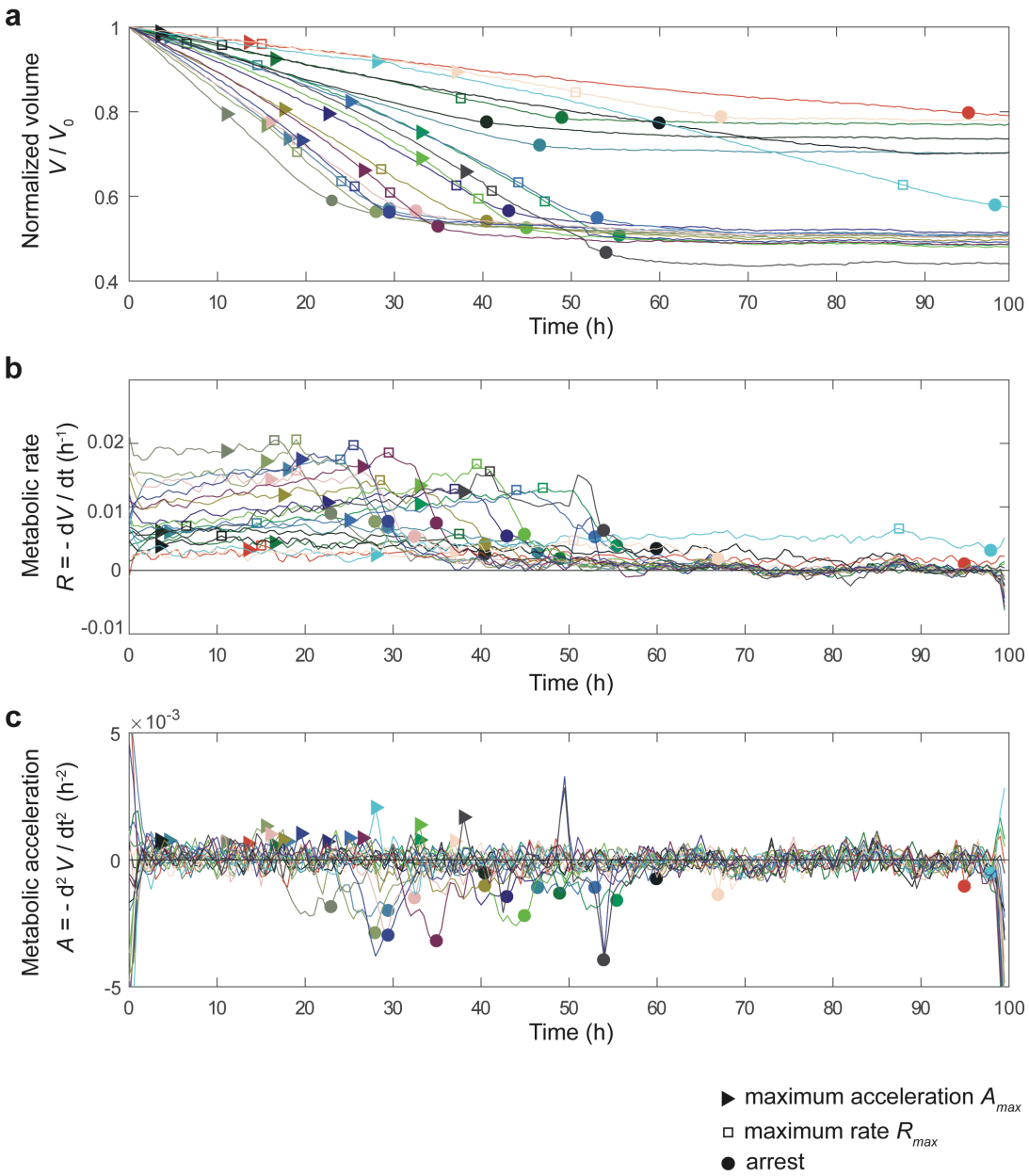

Extended Data Figure 3. Automated analysis of metabolic kinetics from the time-lapse measurement of droplet volumes. a) Example of 20 droplet volumes V over time normalized by their initial volume, V_0. The point of metabolic acceleration (A_{max}) is shown by triangles, of maximum rate (R_{max}) by squares and metabolic arrest (T_{arr}) by circles (see below). b) Metabolic rate R computed as minus the time derivative of the normalized volume. R_{max} (square) is determined as the maximum of each curve. Metabolic arrest is determined as the point at which R reaches 1/10 of R_{max}, and generally corresponds to the minimum of the acceleration curves in panel c, although the latter yields a less reliable estimate. c) Metabolic acceleration A computed as the derivative of the metabolic rate. The time of acceleration (triangle) is determined from the maximum A_{max} of this curve. The time of recovery (T_{rec}) is the time at which A_{max} is reached within the population of cells that significantly increase their metabolism ($\Delta R > \Delta R^*$) (see Fig. 2g and Extended Data Figure 4).

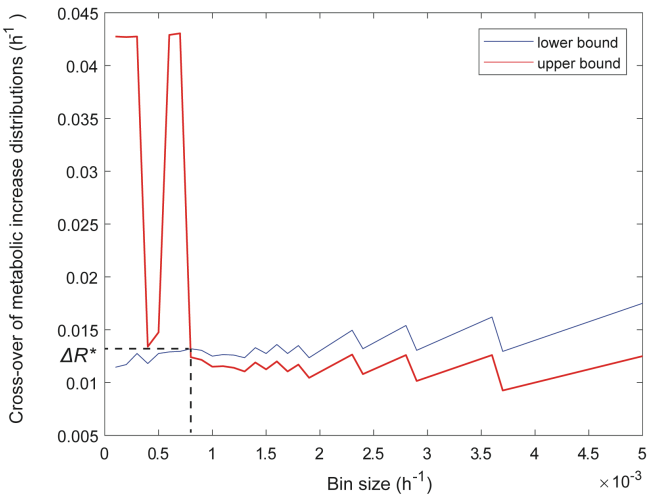

Extended Data Figure 4. Determination of the metabolic increase threshold *ΔR for significant metabolic recovery**. The metabolic increase *ΔR* is the difference between the initial metabolic rate (taken at 2 hours) and the maximum measured metabolic rate R_{max} (see Extended Data Figure 3). For each bin size, we determined the lower and upper bound for the cross-over between the metabolic increase distributions (see Fig. 2g), in the presence or absence of metabolic challenge. These bounds converge at a certain bin value which optimally defines the cross-over *ΔR** between these two distributions.

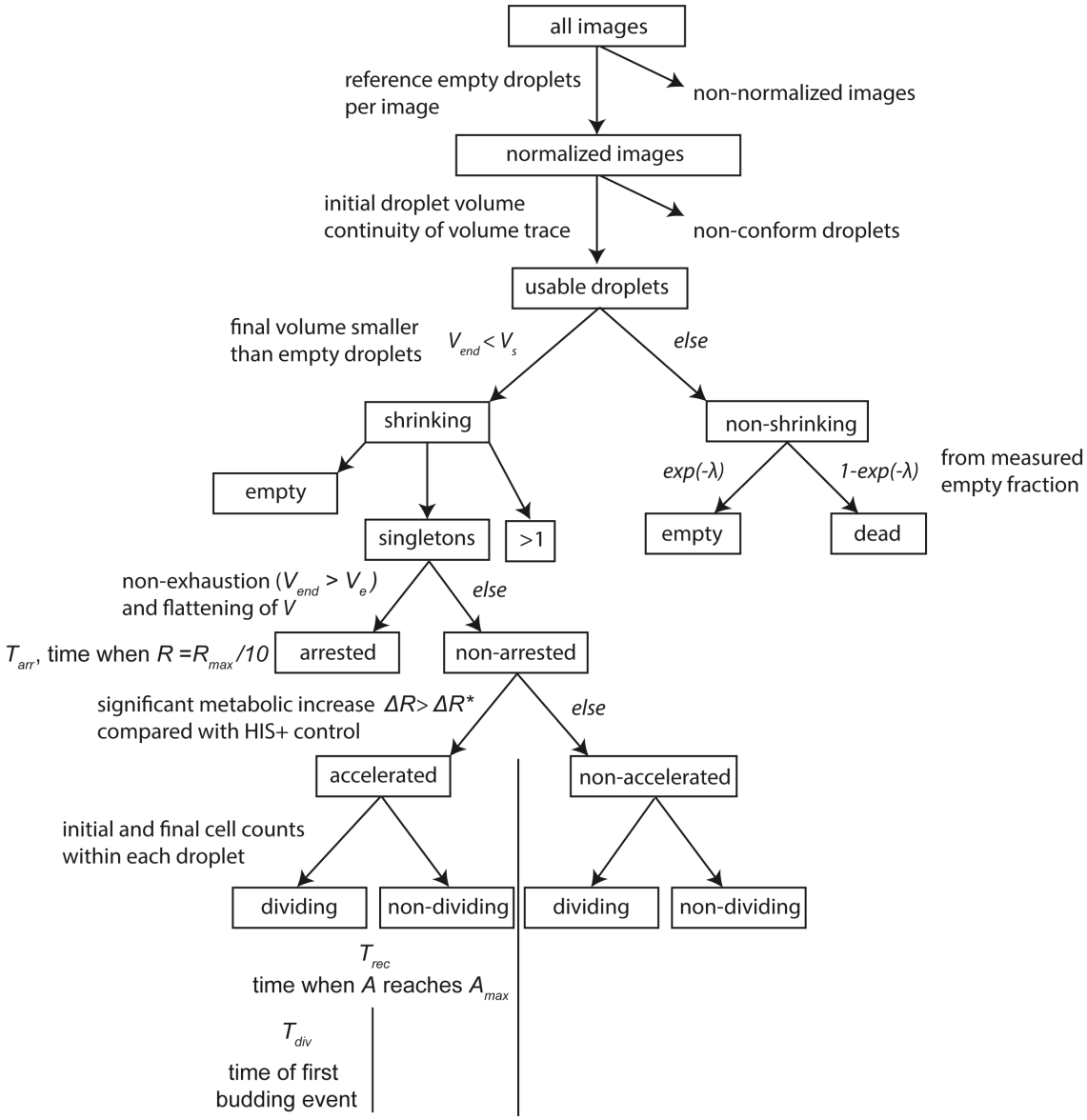

Extended Data Figure 5. Classification tree of metabolic responses. For the details of the treatment, refer to the Methods section "Droplet tracking and quantitative analysis of droplet volumes". V_{end} is the final droplet volume; V_s =1-3σ, where σ is the coefficient of variation of empty droplet final volumes taken over all experiments; V_e is the maximal normalized volume reached by cells in the control experiment (with histidine); λ is the Poisson parameter corresponding to the average number of cells encapsulated per droplet; R is the metabolic rate; R_{max} is the maximum metabolic rate reach for each cell; T_{arr} is the time at which R reaches $R_{max}/10$ in arresting cells; ΔR is the metabolic rate increase computed as the difference between R_{max} and the initial rate R_0 (at 2 hours); ΔR^* is the cross-over value between low and high metabolic rate increases (Extended data Figure 4); A is the metabolic acceleration, which is the time derivate of R; A_{max} is the maximum metabolic acceleration (Extended data Figure 3); T_{rec} is the time at which A_{max} is reached within the population of cells that significantly increase their metabolism ($\Delta R > \Delta R^*$); T_{div} is the time at which the first bud appears in droplets where the final number of cells is larger than 2.

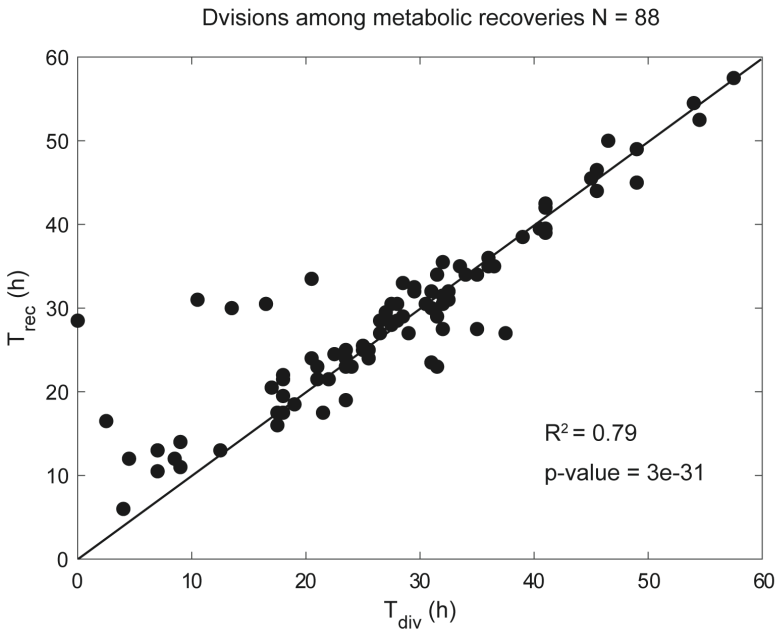

Extended Data Figure 6. Correlation between the times of division (T_{div}) and metabolic recovery (T_{rec}). Each dot corresponds to the analysis of a single volume trace measured in the absence of histidine. The diagonal corresponds to $T_{div} = T_{rec}$.

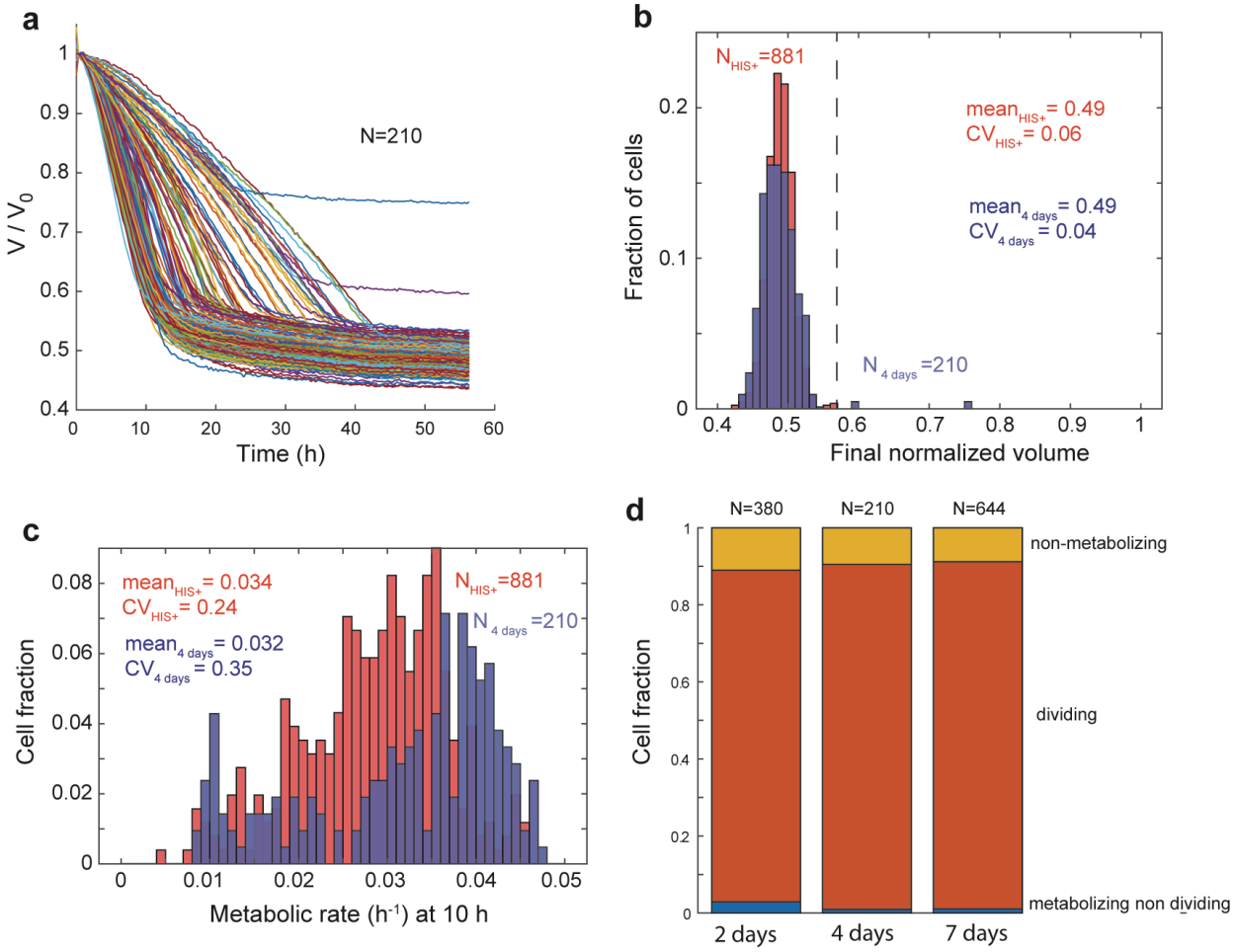

Extended Data Figure 7. Adapted population. a) Volume traces of droplets containing single cells taken from the culture 4 days after the challenge. Droplet volume V is normalized by the initial volume V_0. Lines are color coded as for Fig. 2d. b) Distribution of final volumes (at 70 hours) 4 days after the challenge (blue) and for the control with histidine (red). The vertical dashed line represents V_e, the maximum normalized volume reached by cells in the histidine positive control. c) Distribution of metabolic rates at 10 hours, 4 days after stress (blue) and for the control with histidine (red). d) Fraction of each cell type 2, 4 and 7 days after the challenge.

Methods

Chemicals. All chemicals were purchased from Sigma–Aldrich unless otherwise mentioned.

Strains and culture conditions. The *Saccharomyces cerevisiae* YPH499 strain carries a deletion of the endogenous chromosomal *HIS3* gene and a plasmid containing the divergent *GAL1*/*GAL10* promoters. There is a *HIS3* gene under sole regulation of *GAL1* promoter, and a *GFP* reporter gene under control of the *GAL10* promoter[9]. Cells were grown from colonies on plates in 25 mL of culture medium comprising: 1.7 g/L of yeast nitrogen base without amino acids and ammonium sulfate, 5 g/L ammonium sulfate, 1.4 g/L amino acid dropout powder (without Trp, His, Leu, Ura), 0.004 g/L L-tryptophan, and 0.002 g/L uracil, 20 g/L of galactose or glucose; and incubated at 30°C, shaking at 200 r.p.m. in 100 mL Erlenmeyer flasks. Cultures were diluted every 12h to maintain OD<1.0 (never transferring less than 3.10^6 cells).

Rewired yeast cells, were first grown in a batch culture with galactose medium lacking histidine. The optical density (OD_{600nm}) of the culture was monitored and it was maintained in the exponential phase of growth by serial dilutions for 2 days. The medium was then switched from galactose to glucose. As previously reported[9,14], naïve cells (i.e. rewired cells that had never been grown in glucose before) were able to grow for about 20 hours in glucose media lacking histidine with a doubling time, t_D, of 1.9 h (phase I). Following this phase, the cells ceased growing, or their growth slowed considerably (t_D 17.1 h), leaving the OD_{600nm} approximately constant (phase II, the "latent phase"). At the end of this phase, after durations that varied across repeated experiments from (1 day to 6 days), the population adapted and started growing and proliferating (phase III, the "adapted phase"). The doubling time of the adapted population reduced from 3.1 h 1 day after entering phase III, to 2.1 h after 8 days in phase III (Fig. 1), reflecting the fact that the population continues to adapt after resuming growth[10]. **Microfluidic device fabrication.** Microfluidic devices were obtained using conventional soft lithography methods[31], as described[32]. Molds were prepared using SU8-2015 or SU8-2075 photoresist (MicroChem Corp.) and used to pattern 20 and 75 µm-deep channels onto silicon wafers (Siltronix). The channels of the devices were passivated with Aquapel in HFE7100 (3M) and subsequently flushed with compressed nitrogen gas.

Formation and imaging of droplet arrays. To measure single-cell metabolic and growth dynamics, yeast cells from batch culture were individually compartmentalized in 200,000 monodisperse 30 pL volume (38 µm diameter) aqueous droplets containing fresh glucose medium lacking histidine and incubated at 30°C in a 2D array, taking images every 30 minutes over three days, as described in Boitard et al.[8] Briefly, a flow-focusing device[33] was used for droplet generation and flow rates were controlled using standard-pressure infuse/withdraw PHD 22/2000 syringe pumps (Harvard Apparatus Inc., Holliston, MA). Syringes (Hamilton) connected to the microfluidic device using 0.6 x 25 mm Neolus needles (Terumo Corporation) and PTFE tubing with an internal diameter of 0.56 mm and an external diameter of 1.07 mm (Fisher Bioblock Scientific). The aqueous phase, comprising cells suspended in culture medium, was injected at 300 µL/h and dispersed in a continuous phase consisting of HFE-7500 fluorinated oil (3M) containing 2% (w/w) 008-FluoroSurfactant (RAN Biotechnologies), a PFPE-PEG-PFPE amphiphilic tri-block copolymer[34], injected at 150 µL/h, forming 30 pL volume (38 µm diameter) droplets at 2,800 droplets s^{-1}. Droplets were produced in a compact manner and were directly incubated in a glass chamber of 3.5 x 1.5 cm to form a compact 2D droplet array[8]. Compaction of the emulsion prevents droplet movement to enable their tracking over long

time scales. The chamber was maintained at 30°C on a Nikon T300 inverted microscope with a Thorlabs MAX202 XY stage. Images of the droplet array were taken every 30 min using a Hamamatsu Orca-ER camera. Custom-made Labview software was used to automate image acquisition and microscope control.

Data processing. For a schematic representation see Extended Data Fig. 5.

Droplet tracking and quantitative analysis of droplet volumes. Droplets were detected with an in-house Matlab segmentation routine and tracked in time by a nearest neighbour criterion, knowing that displacements from image to image are much smaller than the characteristic droplet diameter. Images in which large displacements occurred were easily detected as they displayed strongly discontinuous volume traces and were discarded. In order to minimize volume fluctuations caused by defocusing in time, volumes were normalized by the time course of the average of more than 10 empty droplets for each image. Images for which normalization failed were discarded (Extended Data Fig. 5). The Poisson parameter λ (the mean number of cells per droplet) was determined from the frequency of occupied droplets on a sample of 10 initial images (~1500 droplets) per experiment. The number of droplets containing cells arrested from the start was estimated by calculating the difference between λ and the number of significantly shrinking droplets (Extended Data Fig. 5). A droplet was considered to be significantly shrinking is its final normalized volume V_{end} was smaller than V_s =1-3σ, where σ is the coefficient of variation of empty droplet final volumes taken over all experiments (Extended Data Fig. 1). We measured V_s = 0.95. The first and second derivatives of the normalized volume over time were computed over 5 time point sliding windows and provide the metabolic rate R (h^{-1}) and metabolic acceleration A (h^{-2}) (Extended Data Fig. 3). These quantities were used to automatically determine the maximum metabolic rate R_{max}, the metabolic increase ΔR (h^{-1}, difference between the initial metabolic rate R at 2 hours and R_{max}) and the time of maximum metabolic acceleration A_{max}. Metabolically arrested cells were defined as cells: (i) which do not consume all the nutrients available in the droplets within the timeframe of the experiment, as defined by $V_{end} > V_e$, where V_{end} is the final droplet volume and V_e = 0.55 is the maximal normalized volume reached by cells in the control experiment (with histidine), and (ii) for which the volume trace significantly flattens during the time course of the experiment. The latter was determined, within the subpopulation of cells wherein $V_{end} > V_e$, as the existence of an inflection in the volume curve leading to a rate $R < R_{max}/10$ after the maximum rate R_{max} observed for this cell has been reached. The metabolic arrest point (T_{arr}) is defined as the time at which R reaches $R_{max}/10$ (Extended Data Fig. 3). In stress experiments, metabolisms were considered to be significantly accelerating when metabolic increase ΔR was comparably high to that of control cells with histidine $\Delta R_{\mathrm{HIS+}}$. For this we determined the lower and upper bounds of the crossing values for the histograms of ΔR after stress and $\Delta R_{\mathrm{HIS+}}$ as given for different binning intervals. The threshold value ΔR^* = 0.013 h^{-1} was obtained when these bounds converge (Extended Data Fig. 4). For cells classified as significantly increasing their metabolic rate ($\Delta R > \Delta R^*$), the time of metabolic recovery T_{rec} was determined as the time of maximum metabolic acceleration A_{max} (Extended Data Fig. 3c). The time of division T_{div} was determined as the first observed budding event in droplets which contained one cell at the beginning of the experiment and two or more cells at the end of the experiment.

Instantaneous frequencies of arrest and metabolic recovery. Three distinct cell fates were categorized from the metabolic curves: metabolic arrest, metabolic recovery and non-accelerated cells. Calling N the total number of cells observed during the experiment, N_a and N_r the respective

cumulative number of arrested and recovering cells, the instantaneous rate of arrest and recovery were respectively computed as $dN_a/dt/(N - N_a - N_r)$ and $dN_r/dt/(N - N_a - N_r)$. These values were computed both for the experimental data and from their quadratic fit at initial times (0 to 30 hours) (Fig. 4 b and g).

Effective coefficients of determination. The correlations of Figure 4, panels c and h, display regions of experimentally inaccessible parameter values, due to the finite amount of resource available in each droplets and the noise in droplet volume measurements. The coefficient of determination R_a^2 computed directly from the data thus comprises a contribution of these boundary constraints. This contribution R_b^2 to the total covariance has been estimated with a Monte Carlo approach preserving the marginal distributions: 10^5 random permutations of the measured values were generated under the boundary constraints, taking R_b^2 as the mean coefficient of determination of the last 10^4 realizations. Assuming independence between the experimental constraints and cell fates in the absence of resource exhaustion, the additive contribution of these phenomena to the covariance leads to effective coefficients of determinations $R^2 = R_b^2 - R_a^2$.

Characteristic of the characteristic amount of glucose required for a cell to adapt. Adaptation peaked at 74% of the initial volume of 30 pL of droplet with a concentration of 20 g/L of glucose, which leads to a characteristic amount of glucose of $(1 - 0.74) * 30 * 20 = 156$ pg.

References for Methods

31 Xia, Y. N. & Whitesides, G. M. Soft lithography. *Annu Rev Mater Sci* **28**, 153-184 (1998).

32 Frenz, L., Blank, K., Brouzes, E. & Griffiths, A. D. Reliable microfluidic on-chip incubation of droplets in delay-lines. *Lab Chip* **9**, 1344-1348 (2009).

33 Anna, S. L., Bontoux, N. & Stone, H. A. Formation of dispersions using "flow focusing" in microchannels. *Appl Phys Lett* **82**, 364-366 (2003).

34 Holtze, C. *et al.* Biocompatible surfactants for water-in-fluorocarbon emulsions. *Lab Chip* **8**, 1632-1639 (2008).

Supplementary Information

Supplementary Video 1. Droplets were incubated at 30°C in a sealed glass chamber imaged over 70h. Images were taken every 30 min, as indicated by the time stamp. Individual cells were compartmentalised in aqueous droplets dispersed in an oil phase and parked in a 2D array in a closed glass chamber. About 6% of the droplets contain a single cell. The consumption of nutrients (glucose) in a cell-containing droplet creates an osmotic imbalance, resulting in an osmotically driven water flux, which induces the shrinkage of this droplet and the swelling of neighboring cell-free droplets The change in volume of the droplet containing the cell is extracted by image analysis to measure cell metabolism in function of time, while imaging enables measurement of cell division.

Supplementary Table 1. Parameters measured and computed for each individual experiment after stress, after adaptation, for the control with histidine, and over groups of experiments. In all cases, the symbol “N” refers to a number of droplets.